Original Research

Identification of Fibers at Risk for Degeneration by Diffusion Tractography in Patients at High Risk for MS after a Clinically Isolated Syndrome

Jack H. Simon, MD, PhD,[1]* Song Zhang, PhD,[2] David H. Laidlaw, PhD,[2] David E. Miller, PhD,[1] Mark Brown, PhD,[1] John Corboy, MD,[3,4] and Jeffrey Bennett, MD, PhD[3,5]

Purpose: Focal inflammatory/demyelinating lesions are thought to be the source of Wallerian degeneration or other injury to local, transiting fiber tracts in the brain or spinal cord in multiple sclerosis (MS). A methodology is established to isolate connections between focal demyelinating lesions and intersecting fibers to permit explicit analyses of the pathology of secondary fiber injury distant from the focal lesion.

Materials and Methods: A strategy is described and feasibility demonstrated in three patients with a clinically isolated syndrome and positive MRI (at high risk for MS). The strategy utilizes streamtube diffusion tractography to identify neuronal fibers that intersect a focal lesion and pass through a region of interest, in this case the corpus callosum, where distal (to focal lesion) interrogation can be accomplished.

Results: A sizeable fraction of the normal appearing white matter (NAWM) in the early stages of disease can be defined in the corpus callosum, which is distinctive in that this tissue connects to distant demyelinating lesions.

Conclusion: The new class of tissue called fibers-at-risk for degeneration (FAR) can be identified and interrogated by a variety of quantitative MRI methodologies to better understand neuronal degeneration in MS.

Key Words: multiple sclerosis; diffusion; tractography; neuronal degeneration; MRI; inflammation; Wallerian degeneration
J. Magn. Reson. Imaging 2006;24:983–988.
Published 2006 Wiley-Liss, Inc.†

WHILE MULTIPLE SCLEROSIS (MS) is principally considered an inflammatory–demyelinating disease, acute focal inflammatory MS lesions can harbor substantial axonal injury that includes axonal transection (1,2). There is an increasing amount of literature that suggests these focal lesions are the source of Wallerian degeneration or other injury to local, transiting fiber tracts. Evidence for secondary degeneration includes visualization of high signal intensity bands on conventional T2-weighted imaging exit from inflammatory lesions (3,4), in vivo MRI diffusion measures of corpus callosum injury (5–7), and direct measures of fiber loss at autopsy (8). In addition, empty myelin cylinders were observed by confocal microscopy in the cervical spinal cord weeks after a focal brain stem inflammatory–demyelinating event (9).

In theory, a methodology establishing connections between focal demyelinating lesions and intersecting fibers would permit explicit analyses of the pathology of secondary fiber injury. Unfortunately, by conventional two- and even three-dimensional MR imaging, the relationship between focal MS lesions and fiber pathways cannot be accurately determined, and connectivity estimates based on imaging may be misleading. Here, we report a strategy to establish connectivity between focal demyelinating lesions and distant fiber tracts, applied in patients at high risk for MS after a clinically isolated syndrome (CIS). We demonstrate the feasibility of this approach and establish a new class of tissue we call fibers-at-risk (FAR) through connectivity that can be comprehensively interrogated by multiple quantitative MRI methodologies.

MATERIALS AND METHODS

The feasibility of this approach is demonstrated in the first three consecutive patients recruited after informed consent into a prospective longitudinal study of neuronal tract degeneration in early MS. Entry requirements included a CIS involving the optic nerve, spinal cord, or brainstem/cerebellum, and a positive clinical MRI (two or more T2-hyperintense lesions, one periventricular and/or ovoid, with a minimum diameter of 3 mm), which placed these patients at a high risk for ongoing demyelination (10).

[1]Department of Radiology, University of Colorado, Denver, Colorado, USA.
[2]Department of Computer Science, Brown University, Providence, Rhode Island, USA.
[3]Department of Neurology, University of Colorado, Denver, Colorado, USA.
[4]Department of Neurology, Denver Veterans Affairs Medical Center, Denver, Colorado, USA.
[5]Department of Ophthalmology, University of Colorado, Denver, Colorado, USA.

Contract grant sponsor: General Electric Medical Systems; Contract grant sponsor: National MS Society; Contract grant number: RG 3307-A-1; Contract grant sponsor: National Science Foundation; Contract grant number :CCR-0086065.

*Address reprint requests to: J.H.S. MD, PhD, Department of Radiology, Box A-034, University of Colorado Health Sciences Center, 4200 E Ninth Ave, Denver, CO 80262. E-mail: jack.simon@uchsc.edu

Received June 14, 2005; Accepted June 29, 2006.
DOI 10.1002/jmri.20719
Published online 5 October 2006 in Wiley InterScience (www.interscience.wiley.com).

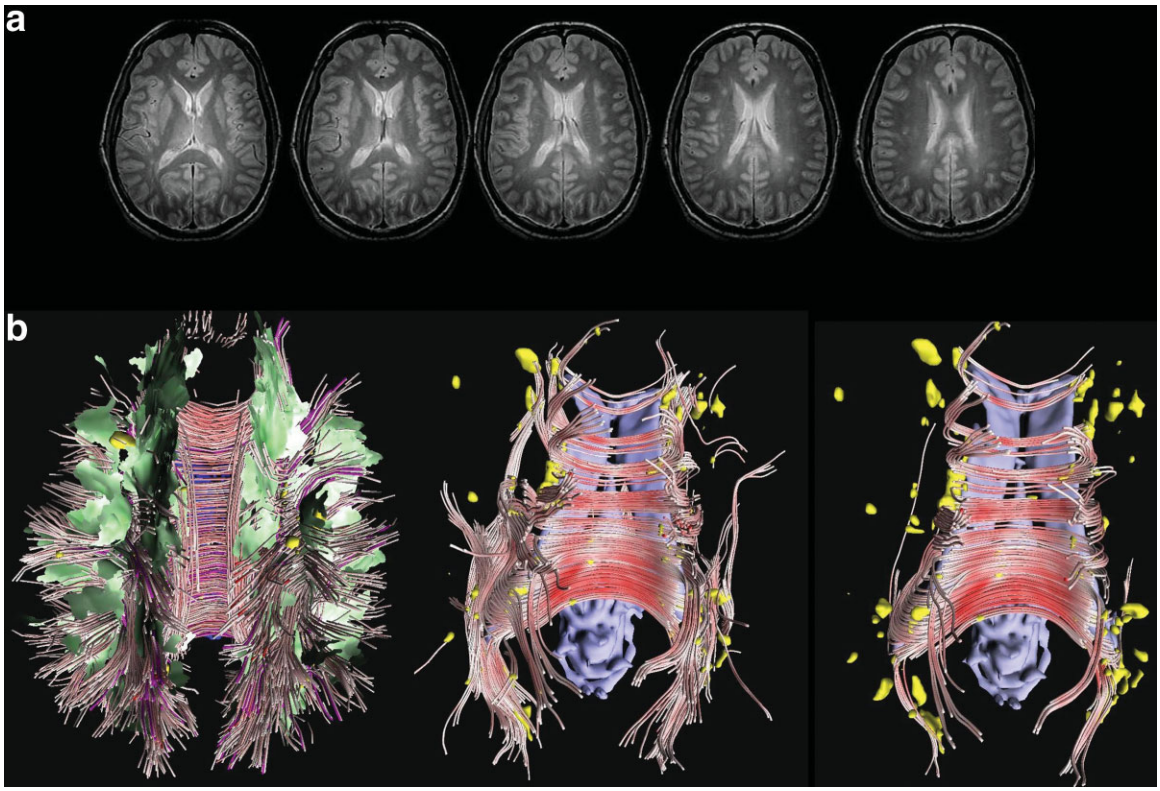

Figure 1.

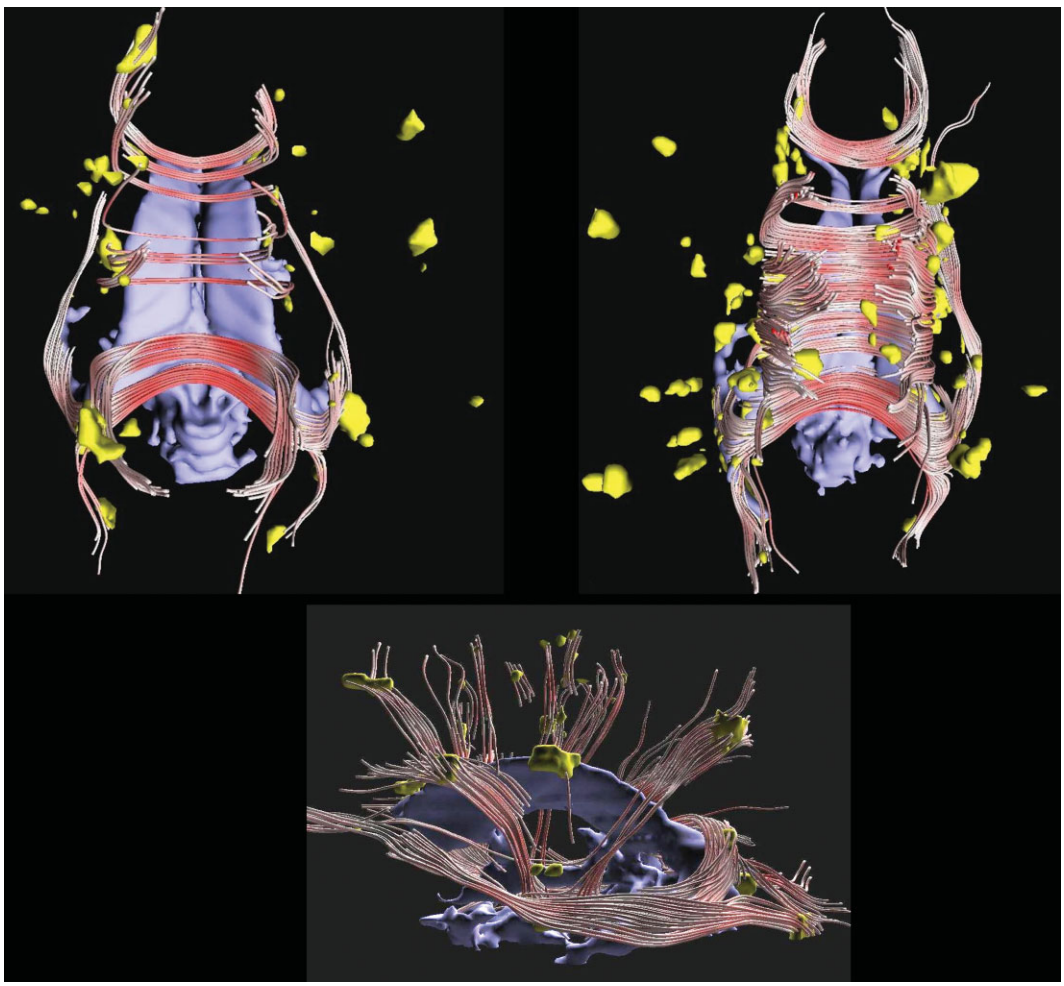

Figure 2.

Table 1
Patient Characteristics

Patient	Age/gender	CIS presentation	DIS	Brain T2 lesion volume (cc)	CDMS	New MR lesions on follow-up?	Treated
1	38/M	Optic neuritis; OCB positive	+	5.83	No	At 3 month	Yes
2	33/F	Partial transverse myelitis	+	2.99	No	At 1 month, 3 month	Yes
3	26/F	Optic neuritis	+	10.69	No	At 1 year	Yes

OCB = oligoclonal bands, DIS = fulfill McDonald criteria for dissemination in space, CDMS = clinically definite MS based on second attack by 1.5-year follow-up, Treated = treatment with immunomodulatory therapy.

A standardized baseline MRI was acquired at 3T with a whole body instrument. MRI sequences included: 1) axial 3-mm-thick nongapped proton density/T2 fast spin echo (FSE) with TR = 4000 msec, $TE_{1,2}$ = 14 and 84 msec, respectively, echo train (ET) = 8, field of view (FOV) = 22 × 22 cm^2, matrix size = 192 × 256, and two excitations; 2) sagittal T2-weighted FSE series with 3-mm-thick nongapped slices, with TR/TE = 6000 msec/110 msec, ET = 15, FOV = 22 × 22 cm, matrix size = 256 × 192, and one excitation; 3) diffusion tensor imaging in the axial plane using an echo-planar sequence with TR/TE = 6075 msec/69.8 msec (minimum), FOV = 28 × 28 cm^2, matrix size = 160 × 160, and two excitations. The maximal b-value was 1000 and 25 gradient directions were acquired. For the diffusion tensor sequence, the slice thickness was 5.1 mm, run three times, each series shifted from the prior by 1.7 mm. By this approach we approximate isotropic three-dimensional sampling, the resulting images can be interpolated in all three coordinate directions nearly equivalently; and 5) a three-dimensional gradient-echo magnetization transfer (MT) pulse sequence was acquired in the sagittal plane with 3-mm partitions, TR/TE/flip angle = 50 msec/2.4 msec/15°, FOV = 22 × 22 cm^2, matrix size = 256 × 192, and one excitation. The MT pulse was a Fermipulse (used to minimize SAR) with a pulse width of 8 msec and a peak B_1 field of 9.24 μT, for a flip angle of 670°, applied 1200 Hz from the center frequency. The MT pulse was applied for every slice-encoding step but only for the middle 30% of the phase-encode steps, to avoid exceeding specific absorptions rate (SAR) restrictions.

Figure 1. Case 1. **a:** Five representative T2-weighted slices show multiple small T2 hyperintense lesions in the vicinity of the corpus callosum. **b:** Culling procedure. Left: Streamtube visualization (view from above) including the full set of streamsurfaces (green) and streamtubes (red) in relation to focal T2-hyperintense lesions (yellow) and ventricle (blue). Middle: Visualization culled to include streamtubes that intersect focal T2-hyperintense lesions. Right: Set of streamtubes fully culled to include fibers intersecting focal T2-hyperintense lesion and crossing corpus callosum. Saturation of colors are used to represent strength of linear anisotropy (redness).

Figure 2. Fully culled images for case 2 (left) and case 3 (right). Bottom is a lateral visualization from case 2. Note the complex curvature of callosal fibers in both the superior–inferior directions (arrow) and anterior–posterior direction (curved arrows), which can be distinguished from other fiber tracts such as those running anterior–posterior (arrow heads).

Total brain T2-hyperintense lesions were determined using the axial proton density/T2 image pairs using the Analysis Application for Medical Imaging (AAMI), an in-house semiautomated analysis application written in the Interactive Data Language (IDL) interpreted programming language (Research Systems, Inc., Boulder, CO; www.rsinc.com). The abnormal appearing white matter (AAWM) fraction of the corpus callosum was based on the central sagittal T2-weighted image using AAMI and expert confirmation. The normal appearing white matter (NAWM) of the corpus callosum was defined on the same slice as the full corpus callosum minus the AAWM fraction on the same image. The corpus callosum area was determined based on lesion/edge-gradient segmentation routines from the same central slice. Segmented data was registered to B_0 space via affine transformations optimized by a mutual information algorithm.

The diffusion tensor was fitted from the acquired diffusion-weighted images for each voxel in the brain using a nonlinear approach (11). Streamtubes and streamsurfaces were generated for visualizing regions of linear diffusion anisotropy area and planar diffusion anisotropy area, respectively (12,13). For analyzing affected neural fibers, we used only the streamtubes model. First, a full set of streamtubes was determined, which represented coherent white matter tracts extending from a dense set of seed points, following the direction of fastest diffusion (the principal eigenvector of the diffusion tensor). The extension was terminated when low linear diffusion or a data boundary was encountered, or when the path curved excessively. This process resulted in about 500,000 streamtubes that were further culled based on length, average diffusion anisotropy, and redundancy (13), leaving about 2000 streamtubes (Fig 1). Next, the subset of streamtubes with seed points within the three-dimensional coordinates of T2-hyperintense lesions was retained. Finally, the set of streamtubes was further culled to retain only those that intersected the corpus callosum.

Tractography was based on a three-dimensional grid defined every 2.2 mm. For each grid point, a small random perturbation was added to the location; the resulting set of points was used to seed integral curves or streamtubes (13). These were created in regions in which linear anisotropy was greater than 0.1. Streamtubes shorter than 5.5 mm or with an average linear anisotropy less than 0.2 were culled. Redundant streamtubes were also culled (two streamtubes were considered redundant if the average distance above 0.5 mm between them was less than 1 m). To get a more

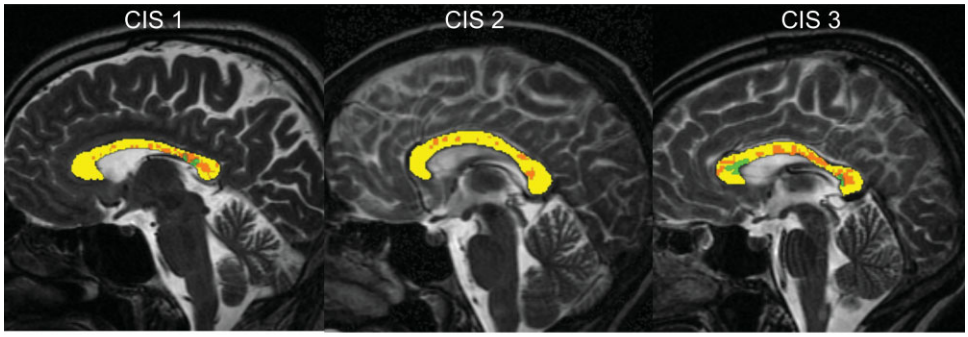

ID	Corpus Callosum Area		Mean MTR			
	FAR %	AAWM %	All Corpus Callosum	NAWM Fraction	AAWM Fraction	FAR Fraction
CIS 1	21.0	4.1	48.94	49.06	45.98	50.57
CIS 2	10.0	0	49.55	49.55		49.78
CIS 3	30.0	8.7	48.53	48.55	48.36	50.63

Figure 3. Coregistered data on sagittal T2-weighted midsagittal images show the tissue classes corpus callosum (yellow), abnormal appearing white matter (green), and FAR in red. Overlapping pixels represented by intensity variation. Note that most of the FAR is not associated with the AAWM fraction. In the chart (bottom), the relative fraction of FAR and AAWM are shown, as well as the MTR values for the three cases.

detailed model in the lesion area, we used a three-dimensional grid defined every 1.1 mm for those FAR models (which were seeded only in the lesion area). The distance thresholds were set so that two streamtubes were considered redundant if the average distance above 0.25 mm between them was less than 0.5 mm.

Streamtube tractography data (acquired using the echo-planar technique) and MT data (acquired by three-dimensional gradient echo) were registered to the T2 space via affine transformation optimized by a mutual information algorithm. Magnetization transfer ratio (MTR) values for FAR regions in the corpus callosum were calculated based on MTR = [Signal Intensity MT_{pre}-Signal Intensity MT_{post}]/[Signal Intensity MT_{pre}] * 100, with MT_{pre} and MT_{post} being the sequences prior to and after addition of the MT pulse.

RESULTS

Patient characteristics are summarized in Table 1. All three patients were treated after diagnosis of CIS and having a high-risk for MS based on a positive MRI (patients 1–3) and oligoclonal bands (patient 1). Over a 1.5 year follow-up, none have had a second clinical attack, but all three showed evidence for ongoing demyelinating activity based on follow-up MRI.

Figure 1a provides representative T2-weighted images showing the number and distribution of focal T2-hyperintense lesions located within the central brain slices. The relationship of these lesions to fiber pathways is completely indeterminate. The culling process to obtain the set of limited neuronal FAR is summarized for patient 1 in Fig. 1. The bottom row left image shows the still complex three-dimensional set of ~2000 (simplified for visualization) streamtubes and streamsurfaces that are derived based on the full data set. Figure 1b (middle) is a considerably more interpretable visualization restricted to fibers intersecting with focal T2-hyperintense lesions, a broad group of FAR for degeneration. Figure 1b (right) shows that set of fibers intersecting T2-hyperintense lesions that pass through the corpus callosum, a more restricted set of FAR.

Figure 2 shows the subset of FAR passing through the corpus callosum in patients 2 and 3. A lateral view selected from the three-dimensional visualization image set in patient 2 shows that the technique is capable of distinguishing fibers with a high degree of specificity based on their anatomic course. This would not be possible by visualizing two-dimensional or even three-dimensional conventional images, since the fibers of all pathways including the corpus callosum follow complex and curving positions in space.

Figure 3 shows a representation of the FAR in corpus callosum in the three patients relative to the NAWM and AAWM. In all cases, while focal MS lesions were common in parasagittal slices including the corpus callosum (not shown), focal lesions were relatively rare in the true central slice of the corpus callosum. FAR through the corpus callosum accounted for 21%, 10%, and 30% of the total corpus callosum midsagittal area in patients 1, 2, and 3, respectively. In contrast, AAWM accounted for a smaller fraction of the central corpus callosum area, at 4.1%, 0%, and 8.7%, in patients 1, 2, and 3, respectively. These data were part of a large set of planned analyses in a prospective study and were not analyzed for statistical significance. However on preliminary examination (Fig. 3), MTR values appear abnormally low in the AAWM fraction, and relatively normal in the FAR and NAWM fractions.

DISCUSSION

The streamtube diffusion tractography strategy described here provides a mechanism for identifying vox-

els in the brain that contain neuronal fibers that are at risk for injury through secondary neuronal degeneration. FAR are distinct from tissue at risk by focal inflammatory/demyelinating pathology, and are distinct from the NAWM tissue fraction. Alternative approaches to relate focal MS lesions to related fiber pathways are limited by the necessity to assume anatomical relationships. Our studies show that even for the relatively well-oriented interhemispheric fibers of the corpus callosum, fibers gracefully curve in three-dimensional space across and through slices, which makes assumptions about spatial relationships inaccurate at best.

This pilot study provides proof-of-concept that the tractography approach provides a unique perspective into early MS pathology. For example, we can visualize the full extent of potentially injured FAR in the corpus callosum. The FAR are distinct from the AAWM, although not unexpectedly there is some overlap. FAR in these "at-risk for" MS cases accounted for 10% to 30% (mean 20%) of the central sagittal corpus callosum area. Based on estimates of about 160 million fibers crossing the adult corpus callosum (14), our series suggests a potential mechanism that places about 32 million fibers already at risk at the time of diagnosis or time of first recognized risk for MS. As the corpus callosum undergoes extensive volume loss early in the disease (15,16), ultimately associated with a striking decrease in neuronal fiber count (8), the large number of FAR, if proven to be injured, may provide insight into the early injury process.

While we do not know at this time if and how the FAR in corpus callosum are injured, there are several lines of evidence suggesting that corpus callosum fiber injury is initiated very early in the disease. Transcallosal bands have been observed based on signal change on T2-weighted imaging in patients at high risk for MS at the time of a CIS (3). These changes are similar in signal pattern to fiber injury in the corticospinal tract (4). While these conventional T2-evident hyperintensities may represent the most severe of a broad range of injuries, those lesions already evident by T2-weighted imaging are likely to be but a small fraction of the total abnormality that would be detected by quantitative MRI methodologies (5–7,17,18).

How much of this injury in the NAWM of the corpus callosum or other NAWM is due to focal microscopic pathology, as opposed to secondary degeneration, is not known, as the quantitative MRI techniques are not specific for the pathology of neuronal degeneration. Loss of diffusion anisotropy, and particularly increased diffusivity perpendicular to the principal fiber direction, findings that are detected in the corpus callosum, are believed to be "signatures" of Wallerian degeneration (7,19,20). In vivo, a regional relationship is found between reduced fractional anisotropy and increased mean diffusivity in the corpus callosum and the separate lesion load in the cerebral lobes (5,6), and atrophy of the corpus callosum is correlated with brain T2 lesion load (21,16). In studies of fixed autopsy specimens, there is a correlation between the regional load of macroscopic lesion in white matter and axonal density and number in the corresponding projection area in the corpus callosum (8).

While we do not see a major decrease in MTR in the FAR in these three cases, this small pilot study was not designed for that purpose, and it is interesting to note that the MTR of the NAWM was likewise not obviously reduced. The relatively normal MTR in FAR and NAWM may be due to a combination of evaluation at an early stage in the disease and the small sample size. Future analyses including evaluation based on the longitudinal series will address the sensitivity of MTR and measures based on diffusion tensor (fractional anisotropy and diffusivity) in this population. It is apparent that noise in the image data and the small size of the tissue fractions of interest may require further optimization of the MRI acquisition, even for studies at 3T where the added signal-to-noise is a benefit compared to conventional imaging ($\leq$1.5T). Fortunately, magnetic susceptibility artifacts including spatial distortions are relatively limited even at 3T in the central brain regions we are evaluating, With regard to the FAR, a potential source of error in our analyses is the possibility for artifactual dropout of visualized fibers related to the known decrease in fractional anisotropy that accompanies the focal pathology in MS (22,23). It is encouraging, however, to note that fibers can be readily traced through and from the surfaces of the focal pathology. Future studies will quantitatively address issues of fiber dropout and the characteristics of the focal pathology associated with more severe fiber dropout.

This FAR strategy is applicable to any neuronal tract that can be imaged with high quality diffusion tensor and structural MRI. In theory, a methodology establishing connections between focal inflammatory and/or demyelinating lesions and intersecting fibers should benefit explicit analyses of the pathology of fiber injury related to individual focal lesions or a composite of all lesions. Such studies could improve our understanding of the temporal relationships of injury and its consequences, the heterogeneity of injury and disease, and potentially provide a basis for assay of neuroprotective therapy.

REFERENCES

1. Ferguson B, Matyszak MK, Esiri MM, Perry VH. Axonal damage in acute multiple sclerosis lesions. Brain 1997;120:393–399.
2. Trapp B, Peterson J, Ransohoff RM, Rudick R, Mörk S, Bö L. Axonal transection in the lesions of Multiple Sclerosis. N Engl J Med 1998; 338:278–285.
3. Simon JH, Jacobs L, Kinkel RP. Transcallosal bands: a sign of neuronal tract degeneration in early MS? Neurology 2001;57:1888–1890.
4. Simon JH, Kinkel RP, Jacobs L, Bub L, Simonian NA. Wallerian degeneration pattern in patients at risk for MS. Neurology 2000;54: 1155–1160.
5. Ciccarelli O, Werring DJ, Barker GJ, et al. A study of the mechanisms of normal-appearing white matter damage in multiple sclerosis using diffusion tensor imaging—evidence of Wallerian degeneration. J Neurol 2003;250:287–292.
6. Ge Y, Law M, Johnson G, et al. Preferential occult injury of corpus callosum in multiple sclerosis measured by diffusion tensor imaging. J Magn Reson Imaging 2004;20:1–7.
7. Henry RG, Oh J, Nelson SJ, Pelletier D. Directional diffusion in relapsing-remitting multiple sclerosis: a possible in vivo signature of Wallerian degeneration. J Magn Reson Imaging 2003;18:420–426.

8. Evangelou N, Konz D, Esiri MM, Smith S, Palace J, Matthews PM. Regional axonal loss in the corpus callosum correlates with cerebral white matter lesion volume and distribution in multiple sclerosis. Brain 2000;123:1845–1849.
9. Bjartmar C, Kinkel RP, Kidd G, Rudick RA, Trapp BD. Axonal loss in normal-appearing white matter in a patient with acute MS. Neurology 2001;57:1248–1252.
10. CHAMPS Study Group. MRI predictors of early conversion to clinically definite MS. Neurology 2002;59:998–1005.
11. Ahrens ET, Laidlaw DH, Readhead C, Brosnan CF, Fraser SE, Jacobs RE. MR microscopy of transgenic mice that spontaneously acquire experimental allergic encephalomyelitis. Magn Reson Med 1998;40:119–132.
12. Westin CF, Maier SE, Mamata H, Nabavi A, Jolesz FA, Kikinis R. Processing and visualization for diffusion tensor MRI. Med Image Anal 2002;6:93–108.
13. Zhang S, Demiralp C, Laidlaw DH. Visualizing diffusion tensor MR images using streamtubes and streamsurfaces. IEEE Trans Vis Comp Graphics 2003;9:454–462.
14. Aboitiz F, Scheibel AB, Fisher RS, Zaidel E. Fiber composition of the human corpus callosum. Brain Res 1992;598:143–153.
15. Simon JH, Jacobs LD, Campion MK, et al. A longitudinal study of brain atrophy in relapsing multiple sclerosis. The Multiple Sclerosis Collaborative Research Group (MSCRG). Neurology 1999;53: 139–148.
16. Pelletier J, Suchet L, Witjas T, et al. A longitudinal study of callosal atrophy and interhemispheric dysfunction in relapsing-remitting multiple sclerosis. Arch Neurol 2001;58:105–111.
17. Ranjeva JP, Pelletier J, Confort-Gouny S, et al. MRI/MRS of corpus callosum in patients with clinically isolated syndrome suggestive of multiple sclerosis. Mult Scler 2003;9:554–565.
18. Coombs BD, Best A, Brown MS, et al. Multiple sclerosis pathology in the normal and abnormal appearing white matter of the corpus callosum by diffusion tensor imaging. Mult Scler 2004;10:392–397.
19. Pierpaoli C, Barnett A, Pajevic S, et al. Water diffusion changes in Wallerian degeneration and their dependence on white matter architecture. Neuroimage 2001;13:1174–1185.
20. Thomalla G, Glauche V, Koch MA, Beaulieu C, Weiller C, Rother J. Diffusion tensor imaging detects early Wallerian degeneration of the pyramidal tract after ischemic stroke. Neuroimage 2004;22: 1767–1774.
21. Simon JH, Schiffer RB, Rudick RA, Herndon RM. Quantitative determination of MS-induced corpus callosum atrophy in vivo using MR imaging. AJNR Am J Neuroradiol 1987;8:599–604.
22. Bammer R, Augustin M, Strasser-Fuchs S, et al. Magnetic resonance diffusion tensor imaging for characterizing diffuse and focal white matter abnormalities in multiple sclerosis. Magn Reson Med 2000;44:583–591.
23. Guo AC, MacFall JR, Provenzale JM. Multiple sclerosis: diffusion tensor MR imaging for evaluation of normal-appearing white matter. Radiology 2002;222:729–736.